

# Current Rectification and Seebeck Coefficient of Serially Coupled Double Quantum Dots

Yen-Chun Tseng and David M.-T. Kuo\*

*Department of Electrical Engineering, National Central University, Chungli 320 Taiwan*

The transport properties of serially coupled quantum dots (SCQDs) embedded in a matrix connected to metallic electrodes are theoretically studied in the linear and nonlinear regimes. The current rectification and negative differential conductance of SCQDs under the Pauli spin blockade condition are attributed to the combination of bias-direction dependent probability weight and off-resonant energy levels yielded by the applied bias across the junctions. We observe the spin-polarization current rectification under the Zeeman effect. The maximum spin-polarization current occurs in the forward bias regime. Such behavior is different from the charge current rectification. Finally, the Seebeck coefficient ( $S$ ) of SCQDs is calculated and analyzed in the cases without and with electron phonon interactions. The application of SCQDs as a temperature detector is discussed on the basis of the nonlinear behavior of  $S$  with respect to temperature difference across the junction.

## 1. Introduction

Serially coupled quantum dots (SCQDs) exhibit the transport properties of current rectification due to the Pauli spin blockade, negative differential conductance (NDC), nonthermal broadening of the tunneling current, and coherent tunneling in the Coulomb blockade regime.<sup>1–3</sup> Although many theoretical works have been devoted to investigating these phenomena, they still can not explain the transport properties of SCQDs systematically.<sup>4–8</sup> Sun et al calculated the tunneling current of SCQDs in the Pauli spin blockade using the Keldysh-Green function technique.<sup>4</sup> The procedure introduced in ref [4] to solve high-order Green functions arising from electron Coulomb interactions can not resolve the quantum paths of SCQDs. In Refs. 5–8, the master equation was used to calculate the tunneling current of SCQDs. However, in these works, cases are restricted to  $t_c \ll \Gamma$ , where  $t_c$  and  $\Gamma$  denote, respectively, the interdot hopping strength and tunneling rate between the electrodes and the quantum dots (QDs).

Here, a closed-form expression for the tunneling current of SCQDs with a finite interdot hopping strength enables the analysis of current rectification arising from coherent tunneling with a spin blockade and the NDC of tunneling current resulting from off-resonant energy levels. The effect of Zeeman energy splitting on tunneling current is investigated to clarify the behavior of spin-polarization current. In addition, the Seebeck coefficient ( $S$ ) of SCQDs is calculated in the cases without and with electron phonon interactions (EPIs). In the absence of EPIs, we propose how to use SCQDs as a temperature detector on the basis of the nonlinear Seebeck coefficient. When the SCQDs are embedded in a phonon cavity<sup>9–11</sup>, it is possible to manipulate EPIs to control the electrical conductance and Seebeck coefficient of junction systems.

## 2. Formalism

Because we consider nanoscale semiconductor QDs, the energy level separation of between QDs is much larger than their on-site Coulomb interactions and thermal energies. One energy level for each quantum dot is con-

sidered in this study. The two-level Anderson model including EPIs is employed to simulate the SCQD junction system shown in the inset of Fig. 1(a). The Hamiltonian of an SCQD junction<sup>12</sup> is given by  $H = H_0 + H_{CQD} + H_T$

$$H_0 = \sum_{k,\sigma} \epsilon_k a_{k,\sigma}^\dagger a_{k,\sigma} + \sum_{k,\sigma} \epsilon_k b_{k,\sigma}^\dagger b_{k,\sigma} \quad (1)$$

$$+ \sum_{k,\sigma} V_{k,1} d_{1,\sigma}^\dagger a_{k,\sigma} + \sum_{k,\sigma} V_{k,2} d_{2,\sigma}^\dagger b_{k,\sigma} + c.c$$

where the first two terms describe the free electron gas of the left and right metallic electrodes.  $a_{k,\sigma}^\dagger$  ( $b_{k,\sigma}^\dagger$ ) creates an electron with momentum  $k$  and spin  $\sigma$  with energy  $\epsilon_k$  in the left (right) metallic electrode.  $V_{k,\ell}$  ( $\ell = 1, 2$ ) describes the coupling between the metallic electrodes and the first (second) QD.  $d_{\ell,\sigma}^\dagger$  ( $d_{\ell,\sigma}$ ) creates (destroys) an electron in the  $\ell$ -th dot.

$$H_{CQD} = \sum_{\ell,\sigma} E_\ell n_{\ell,\sigma} + \sum_{\ell} U_\ell n_{\ell,\sigma} n_{\ell,\bar{\sigma}} \quad (2)$$

$$+ \frac{1}{2} \sum_{\ell,j,\sigma,\sigma'} U_{\ell,j} n_{\ell,\sigma} n_{j,\sigma'} + \sum_{\ell,j,\sigma} t_{\ell,j} d_{\ell,\sigma}^\dagger d_{j,\sigma},$$

where  $E_\ell$  is the spin-independent QD energy level and  $n_{\ell,\sigma} = d_{\ell,\sigma}^\dagger d_{\ell,\sigma}$ . Notations  $U_\ell$  and  $U_{\ell,j}$  describe the intradot and interdot Coulomb interactions, respectively.  $t_{\ell,j}$  describes the electron interdot hopping.  $H_T$  describes the EPIs

$$H_T = \omega_0 c^\dagger c + \sum_{\ell,\sigma} \Omega_\ell n_{\ell,\sigma} (c^\dagger + c), \quad (3)$$

where  $\omega_0$  is the phonon cavity frequency and  $\Omega_\ell$  is the coupling strength of EPIs. A canonical transformation can be carried out to remove on-site EPIs, that is,  $H_{new} = e^{S^\dagger} H e^S$ , where  $S = -\sum_{\ell,\sigma} \Omega_\ell n_{\ell,\sigma} (c^\dagger - c)$ .<sup>13,14</sup> In the new Hamiltonian, we have the following effective physical parameters:  $V_{k,1}^e = V_{k,1} e^{\lambda_1 (c^\dagger - c)}$ ,  $V_{k,2}^e =$

$V_{k,2}e^{\lambda_2(c^\dagger - c)}$ ,  $E_\ell^e = E_\ell - \lambda_\ell^2\omega_0$ ,  $U_\ell^e = U_\ell - 2\lambda_\ell^2\omega_0$ ,  $U_{\ell,j}^e = U_{\ell,j} - 2\lambda_1\lambda_2\omega_0$ ,  $t_{\ell,j}^e = t_{\ell,j}e^{-(\lambda_\ell - \lambda_j)(c^\dagger - c)}$ , and  $\lambda_\ell = \Omega_\ell/\omega_0$ . Under the canonical transformation, the coupling strengths between the electrodes and the dots, on-site energy levels, intradot Coulomb interactions, interdot Coulomb interactions, and electron interdot hopping strengths are renormalized by EPIs. If we consider a special case of  $\lambda_1 = -\lambda_2 = \lambda$ , we have

$$H_T = \omega_0 c^\dagger c + \sum_\sigma \Omega(n_{1,\sigma} - n_{2,\sigma})(c^\dagger + c). \quad (4)$$

This special case of Eq. (4) was already considered in refs 15 and 16. For the case of Eq. (4), we have an effective electron interdot Coulomb interaction  $U_{\ell,j} + 2\lambda^2\omega_0$ , which is always repulsive and enhanced with increasing EPIs.<sup>16)</sup>

To decouple the EPIs of  $H_{new}$ , we take the mean-field average to remove the phonon field arising from  $c^\dagger - c$ , which is  $\langle \exp^{\lambda_\ell(c^\dagger - c)} \rangle = \exp^{-\frac{1}{2}\lambda_\ell^2 \coth^2[\omega_0/(2k_B T_p)]}$ . On the basis of such a mean-field average, we see a reduction of  $V_{k,\ell} \exp^{-\frac{1}{2}\lambda_\ell^2 \coth^2[\omega_0/(2k_B T_p)]} = V_{k,\ell} X_\ell$  and interdot hopping strength  $t_{c,\ell} \exp^{-\frac{1}{2}(\lambda_1 - \lambda_2)^2 \coth^2[\omega_0/(2k_B T_p)]} = t_c X_{\ell,j}$ . This leads to the redefinition of the renormalized resonance width of each energy level of the QD.  $T_p$  is the phonon temperature.

Using the Keldysh-Green function technique and neglecting the phonon-assisted tunneling process,<sup>12)</sup> the tunneling current of an SCQD is given by

$$J = \frac{2e}{h} \int d\epsilon \mathcal{T}(\epsilon) [f_L(\epsilon) - f_R(\epsilon)], \quad (5)$$

where  $\mathcal{T}(\epsilon) \equiv (\mathcal{T}_{12}(\epsilon) + \mathcal{T}_{21}(\epsilon))/2$  is the transmission factor.  $f_{L=1(R=2)}(\epsilon) = 1/[e^{(\epsilon - \mu_{L(R)})/k_B T_{L(R)}} + 1]$  denotes the Fermi distribution function for the left (right) electrode. The left (right) chemical potential is given by  $\mu_L(\mu_R)$ .  $\mu_L - \mu_R = e\Delta V_a$ , where  $\Delta V_a$  denotes the applied bias. Notation  $T_{L(R)}$  denotes the equilibrium temperature of the left (right) electrode.  $e$  and  $h$  denote the electron charge and Planck's constant, respectively.  $\mathcal{T}_{\ell,j}(\epsilon)$  denotes the transmission coefficient, which can be calculated by the on-site retarded Green function and the lesser Green function. The transmission coefficient has the following expression:

$$\mathcal{T}_{\ell,j}(\epsilon) = -2 \sum_{m=1}^8 \frac{\Gamma_\ell^e(\epsilon) \Gamma_j^{e,m}(\epsilon)}{\Gamma_\ell^e(\epsilon) + \Gamma_j^{e,m}(\epsilon)} \text{Im} G_{\ell,m,\sigma}^r(\epsilon), \quad (6)$$

where  $\text{Im}$  means taking the imaginary part of the function that follows, and

$$G_{\ell,m,\sigma}^r(\epsilon) = p_m/(\mu_\ell - \Sigma_m). \quad (7)$$

$\Gamma_{\ell=L(1),R(2)}^e(\epsilon) = \Gamma_\ell X_\ell^2$ , where  $\Gamma_\ell = \sum_k V_{k,\ell}^2 \delta(\epsilon - \epsilon_k)$  denotes the tunnel rate from the left electrode to dot A ( $E_1$ ) and from the right electrode to dot B ( $E_2$ ), which is assumed to be energy- and bias-independent for simplicity.  $\mu_\ell = \epsilon - E_\ell^e + i\Gamma_\ell^e/2$ . We can assign the following physical meaning to Eq. (6). The sum in Eq. (6)

is over eight possible configurations labeled by  $m$ . We consider an electron (of spin  $\sigma$ ) entering level  $\ell$ , which can be either occupied (with probability  $N_{\ell,\bar{\sigma}}$ ) or empty (with probability  $1 - N_{\ell,\bar{\sigma}}$ ). For each case, the electron can hop to level  $j$ , which can be empty (with probability  $a_j = 1 - N_{j,\sigma} - N_{j,\bar{\sigma}} + c_j$ ), singly occupied in a spin  $\bar{\sigma}$  state (with probability  $b_{j,\bar{\sigma}} = N_{j,\bar{\sigma}} - c_j$ ) or spin  $\sigma$  state (with probability  $b_{j,\sigma} = N_{j,\sigma} - c_j$ ), or in a double-occupied state (with probability  $c_j$ ). Thus, the probability factors associated with the eight configurations appearing in Eq. (6) are  $p_1 = (1 - N_{\ell,\bar{\sigma}})a_j$ ,  $p_2 = (1 - N_{\ell,\bar{\sigma}})b_{j,\bar{\sigma}}$ ,  $p_3 = (1 - N_{\ell,\bar{\sigma}})b_{j,\sigma}$ ,  $p_4 = (1 - N_{\ell,\bar{\sigma}})c_j$ ,  $p_5 = N_{\ell,\bar{\sigma}}a_j$ ,  $p_6 = N_{\ell,\bar{\sigma}}b_{j,\bar{\sigma}}$ ,  $p_7 = N_{\ell,\bar{\sigma}}b_{j,\sigma}$ , and  $p_8 = N_{\ell,\bar{\sigma}}c_j$ .  $\Sigma_m$  in the denominator of Eq. (7) denotes the self-energy correction due to Coulomb interactions and coupling with level  $j$  (which couples with the other electrode) in configuration  $m$ . We have  $\Sigma_1 = t^2/\mu_j$ ,  $\Sigma_2 = U_{\ell,j}^e + t^2/(\mu_j - U_j^e)$ ,  $\Sigma_3 = U_{\ell,j}^e + t^2/(\mu_j - U_{j,\ell}^e)$ ,  $\Sigma_4 = 2U_{\ell,j}^e + t^2/(\mu_j - U_j^e - U_{j,\ell}^e)$ ,  $\Sigma_5 = U_\ell^e + t^2/(\mu_j - U_{j,\ell}^e)$ ,  $\Sigma_6 = U_\ell^e + U_{\ell,j}^e + t^2/(\mu_j - U_j^e - U_{j,\ell}^e)$ ,  $\Sigma_7 = U_\ell^e + U_{\ell,j}^e + t^2/(\mu_j - 2U_{j,\ell}^e)$ , and  $\Sigma_8 = U_\ell^e + 2U_{\ell,j}^e + t^2/(\mu_j - U_j^e - 2U_{j,\ell}^e)$ . Note that  $t = t_c^e = t_c X_{\ell,j}$ . Here  $\Gamma_j^{e,m} = -2\text{Im}\Sigma_j$  denotes the effective tunneling rate from level  $l$  to the other electrode through level  $j$  in configuration  $m$ . For example,  $\Gamma_j^{e,1} = -2\text{Im}t^2/\mu_j = t^2\Gamma_j^e/[(\epsilon - E_j^e)^2 + (\Gamma_j^e/2)^2]$ . It is noted that  $\Gamma_j^{e,m}$  has the numerator  $\Gamma_j^e$  for all configurations. Furthermore,  $G_{\ell,\sigma}^r(\epsilon) = \sum_{m=1}^8 G_{\ell,m,\sigma}^r(\epsilon)$  is simply the on-site single-particle retarded Green function for level  $\ell$  as given in Eq. (A16) in Ref. 12, and  $G_{\ell,m,\sigma}^r(\epsilon)$  corresponds to its partial Green function in configuration  $m$ .

The probability factors of Eq. (7) are determined by the thermally averaged one-particle occupation number and two-particle correlation functions, which can be obtained by solving the on-site lesser Green functions:<sup>12)</sup>

$$N_{\ell,\sigma} = - \int \frac{d\epsilon}{\pi} \sum_{m=1}^8 \frac{\Gamma_\ell^e f_\ell(\epsilon) + \Gamma_j^{e,m} f_j(\epsilon)}{\Gamma_\ell^e + \Gamma_j^{e,m}} \text{Im} G_{\ell,m,\sigma}^r(\epsilon), \quad (8)$$

and

$$c_\ell = - \int \frac{d\epsilon}{\pi} \sum_{m=5}^8 \frac{\Gamma_\ell^e f_\ell(\epsilon) + \Gamma_j^{e,m} f_j(\epsilon)}{\Gamma_\ell^e + \Gamma_j^{e,m}} \text{Im} G_{\ell,m,\sigma}^r(\epsilon). \quad (9)$$

Note that  $\ell \neq j$  in Eqs. (6), (8) and (9), which are valid under the condition of  $t_c/U_\ell \ll 1$ . We will study the transport properties of SCQDs on the basis of Eqs. (5), (8), and (9).

### 3. Results and discussion

#### 3.1 Current rectification

To numerically calculate the tunneling current of SCQDs without EPIs ( $\lambda_1 = \lambda_2 = 0$ ), we adopt the intradot Coulomb interactions of  $U_\ell = U$  and tunneling rates of  $\Gamma_L = \Gamma_R = \Gamma$ . We consider these conditions of homogenous intradot electron Coulomb interactions, and symmetrical tunneling rates for simplicity. All energy

scales are considered in units of  $\Gamma_0$ . On the other hand,  $\eta_{1(2)}e\Delta V_a$  is employed to describe the energy shift arising from the applied bias  $\Delta V_a$  across the junction. That means that  $E_\ell$  is replaced by  $\epsilon_\ell = E_\ell + \eta_\ell e\Delta V_a$ , assuming the right electrode is grounded. On the basis of the experiment in Ref. 1, we adopt  $\eta_1 = 0.6$  and  $\eta_2 = 0.4$ . Although the factor  $\eta_\ell$  depends on the QD shape, material dielectric constant, and location, we assume that  $\eta_\ell$  is determined by the QD location, that is  $\eta_\ell = L_\ell/L$ , where  $L_\ell$  is the distance between the grounded electrode and the  $\ell$ th QD, and  $L$  is the separation distance between the left electrode and the right electrode.

We plot the tunneling current of SCQDs under the Pauli spin blockade condition ( $E_1 + U_{12} = E_2 + U_2$ ) shown in the inset of Fig. 1(a) for three different interdot Coulomb interactions at  $k_B T = 1 \Gamma_0$ ,  $t_c = 0.1 \Gamma_0$ ,  $U = 30 \Gamma_0$ , and  $\Gamma = \Gamma_0$ . The three curves correspond to (a)  $U_{12} = 0$  and  $E_1 = E_F$ , (b)  $U_{12} = 5 \Gamma_0$  and  $E_1 = E_F - 5 \Gamma_0$ , and (c)  $U_{12} = 10 \Gamma_0$  and  $E_1 = E_F - 10 \Gamma_0$ .  $E_F$  denotes the Fermi energy of the electrodes. The current rectification and negative differential conductance (NDC) of SCQDs are observed. The maximum tunneling current is suppressed in the presence of interdot Coulomb interactions. We note that the  $J_{max,R}/J_{max,F}$  ratios are near 2.  $J_{max,R}$  and  $J_{max,F}$  are the maximum current in the backward bias and forward bias, respectively.  $J_{max,R}/J_{max,F} = 2$  is in very good agreement with an experimental observation.<sup>1</sup> The results shown in Fig. 1 indicate that the Pauli spin blockade condition is not attributed to interdot Coulomb interactions, but to intradot Coulomb interactions. On the basis of Eq. (6), the Pauli spin blockade resonant channel of  $E_1 + U_{12} = E_2 + U_2$  is determined from the probability weights of  $p_2 = (1 - N_{1,\bar{\sigma}})(N_{2,\bar{\sigma}} - c_2)$  and  $p_5 = N_{2,\bar{\sigma}}(1 - N_{1,\bar{\sigma}} - N_{1,\sigma} + c_1)$ , which result from  $\mathcal{T}_{12}$  and  $\mathcal{T}_{21}$ , respectively. Figure 1(b) shows the occupation number  $N_{1(2),\bar{\sigma}} = N_{1(2),\sigma} = N_{1(2)}$  and two particle correlation functions  $c_{1(2)}$  for  $U_{12} = 10\Gamma_0$ . The  $p_2$  of  $\mathcal{T}_{12}$  and  $p_5$  of  $\mathcal{T}_{21}$  are also plotted as indicated by the dotted line and dashed line in Fig. 1(b), respectively. Because  $J_{max,F}$  and  $J_{max,R}$  occur, respectively, at  $e\Delta V_a = 3\Gamma_0$  and  $e\Delta V_a = -4.5\Gamma_0$ , we have  $p_2 = 0.28$  and  $p_5 = 0.3$  at  $e\Delta V_a = 3\Gamma_0$  and  $p_2 = 0.24$  and  $p_5 = 0.65$  at  $e\Delta V_a = -4.5\Gamma_0$ . Their sum is  $p_2 + p_5 = 0.58$  at  $J_{max,F}$  and  $p_2 + p_5 = 0.89$  at  $J_{max,R}$ . This demonstrates why  $J_{max,R}$  is larger than  $J_{max,F}$ . In the reversed bias, the increase in  $p_5$  with respect to  $e\Delta V_a$  results from the enhancement of  $(1 - N_{1,\bar{\sigma}} - N_{1,\sigma} + c_1)$  (dot A empty), which provides an increased probability of tunneling of electrons in the right electrode. This result of  $p_5$  approaching one in the high backward bias indicates that the current spectra shown in Fig. 1(a) are determined not only by the probability weights of  $p_2$  and  $p_5$  but also by off-resonant energy levels. We find that the off-resonant energy level is a key reason to observe the NDC behavior of SCQDs. As a consequence, the QD energy level broadening will significantly influence the maximum currents in the forward and reversed biases.<sup>3</sup> It is worth noting that the

phonon-assisted tunneling process arising from EPIs can not be ignored in the high bias regime.<sup>7</sup> Some current structures of SCQDs<sup>1</sup> in the high-bias regime can be well explained by the phonon-assisted tunneling process.<sup>7</sup>

For the applications of SCQDs in spintronics, it is crucial to measure the spin configuration of each electron in individual QDs. SCQDs have a functionality of spin-charge conversion.<sup>1-3</sup> However, it is not easy to measure the small magnitude of tunneling current in the weak interdot coupling limit of  $t_c/\Gamma \ll 1$ . Although tunneling current can be enhanced by increasing  $t_c$ , we consider how the behavior of current rectification is influenced for  $t_c/\Gamma \approx 1$ . To clarify the above question, we plot the tunneling current of SCQDs at various  $t_c$  values in Figs. 2(a)-2(c). Other physical parameters are the same as those for the curve with  $U_{12} = 10\Gamma_0$  shown in Fig. 1(a). The maximum currents labeled  $J_{max,F}$  and  $J_{max,R}$  are shifted toward a higher bias when  $t_c$  increases. The  $J_{max,R}/J_{max,F}$  ratio slightly decreases. The three maximum currents are  $J_{max,F} = 10.4, 167.8$ , and  $328$ , which correspond to  $e\Delta V_a = 3, 3.6$ , and  $4.8 \Gamma_0$ , respectively. ( $J_{max,R} = 21.6, 319$ , and  $599$  correspond to  $-4.5, -5.6$ , and  $-7.4\Gamma_0$ , respectively). The dashed lines shown in Figs. 2(a)-2(c) show the contributions arising from only the resonant channels  $\Pi_2$  of  $\mathcal{T}_{12}$  and  $\Pi_5$  of  $\mathcal{T}_{21}$ . These dashed lines very close the solid lines at the small applied bias (between  $J_{max,F}$  and  $J_{max,R}$ ) but not at the large applied bias. From the results shown in Figs. 2(a)-2(c), the contributions of  $\Pi_2$  and  $\Pi_5$  still dominate the trend of current spectra. These two resonant channels  $\Pi_2$  and  $\Pi_5$  have the two poles  $\epsilon_\pm = E_F + 0.5e\Delta V_a + i\Gamma/2 \pm 0.5\sqrt{(0.2e\Delta V_a)^2 + 4t_c^2}$ . Their bias-dependent probability weights  $p_2 = (1 - N_{1,\bar{\sigma}})(N_{2,\bar{\sigma}} - c_2)$  and  $p_5 = N_{2,\bar{\sigma}}(1 - N_{1,\bar{\sigma}} - N_{1,\sigma} + c_1)$  are determined by the occupation numbers shown in Figs. 2(d)-2(f). The effect of interdot hopping on  $N_1$  and  $N_2$  is enhanced with increasing  $t_c$ . The results shown in Fig. 2 indicate that the current rectification behavior of the SCQD is not destroyed under the condition of  $t_c/\Gamma \approx 1$ .

Although the SCQD system has the functionality of spin filters under the Pauli spin blockade condition, the tunneling currents in Figs. 1 and 2 do not exhibit the spin-polarization current. The spin-polarization current of SCQDs was theoretically studied in Ref. 4 in which the authors considered the spin-bias and ferromagnetic electrodes. Our study introduces the Zeeman effect arising from a local magnetic field to yield the spin-polarization current under the Pauli spin blockade condition of  $E_1 + U_{12} = E_2 + U_2$ . Here the energy level of each QD depends on electron spin. That is,  $E_{\ell,\sigma} = E_\ell \pm g_\ell \mu_B B \sigma = E_\ell \mp \Delta_{Z,\ell,\sigma}$  is considered, where  $g_\ell$  denotes the  $g$ -factor,  $\mu_B$  is the Bohr magneton, and  $B$  is the magnetic field. For simplicity, we assume the homogenous  $g$  factor  $g_\ell = g < 0$ . We plot the spin-dependent charge current  $J_\sigma$  ( $J_{-\sigma}$ ) and spin-polarization current  $J_p = J_\sigma - J_{-\sigma}$  in Fig. 3. Other physical parameters are the same as those for the curve of  $U_{12} = 10\Gamma_0$  shown in Fig. 1. The increase in spin-polarization cur-

rent is observed with increasing Zeeman splitting. Unlike charge current, the maximum spin-polarization current in the forward bias is larger than that in the backward bias. That is  $J_{p,max,F} > J_{p,max,B}$ . Figure 3(c) shows the spin-dependent probability weights. So far, we have considered  $T_L = T_R = T$  in Figs. 1-3, where the charge currents are generated only by the applied bias. To study the thermoelectric effect of SCQDs, we will consider the case of  $T_L \neq T_R$  to investigate the Seebeck coefficient.

### 3.2 Seebeck coefficient

If the SCQD junction system is in an open circuit, an electrochemical potential will form in response to a temperature difference across junction [see Eq. (5)]; this electrochemical potential is known as the Seebeck voltage (Seebeck effect). The Seebeck coefficient (amount voltage generated per unit temperature gradient) is defined as  $S = \Delta\mu/\Delta T$ , where  $\Delta\mu = \mu_L - \mu_R = e\Delta V_a$  and  $\Delta T = T_L - T_R$  are the voltage difference and temperature difference across the junction, respectively. Recently, many studies have been devoted to the investigation of the thermoelectric effects of SCQDs in the linear response regime.<sup>17-18</sup> Because the efficiency of thermoelectric devices can be enhanced with a large temperature difference,<sup>19</sup> it is important to clarify the behavior of the Seebeck coefficient at a large temperature difference  $\Delta T$ . Previous studies focused on the nonlinear thermoelectric properties of individual QD systems,<sup>20,21</sup> which may not be readily realized from the experimental point of view. The thermal resistivity of the SCQD junction system can be larger than that of a single QD system. This feature allows the SCQD system to maintain a relatively large temperature difference across the junction. In this section, we study the Seebeck coefficient in the linear and nonlinear regimes. An analytical solution of  $S$  in the linear response regime gives useful guidelines for understanding the behavior of  $S$  in the nonlinear response regime.

In the linear response regime, Eq. (5) can be rewritten as  $J = L_0 e \Delta V_a + L_1 k_B \Delta T$ . The thermoelectric coefficient  $L_n$  is given by

$$L_n = \frac{2e}{h} \int d\epsilon \mathcal{T}(\epsilon) \frac{(\epsilon - E_F)^n}{4 \cosh^2((\epsilon - E_F)/(2k_B T))}, \quad (10)$$

where the transmission coefficient  $\mathcal{T}(\epsilon)$  is calculated under the equilibrium condition. We define  $S(T) = \Delta V_a/\Delta T = (k_B/e)(-L_1/L_0)$ . Figure 4 shows the Seebeck coefficient ( $S$ ) of SCQDs with identical QDs as a function of temperature at various QD energy levels  $E_0 - E_F = \Delta = 20, 30, 40, 50 \Gamma_0$ . The negative  $S$  indicates that the diffusion electrons pass through the resonant channels of  $E_0 \pm t_c$ ,  $E_0 + U_{12} \pm t_c$ ,  $E_0 + U + U_{12} \pm t_c$ , and  $E_0 + U + 2U_{12}$ . These resonant channels result from the four configurations of  $p_1$ ,  $p_3$ ,  $p_6$ , and  $p_8$  in Eq. (7). The maximum  $S(T_0)$  increases with increasing  $\Delta$ .  $T_0$  denotes the temperature at which  $S$  has a maximum value. In addition,  $T_0$  is shifted toward the high-temperature regime. The dashed lines calculated using

$S_0(T) = -\Delta/T$  are employed to fit these solid lines. These fitting curves show good agreement with the solid lines in the high-temperature regime. The characteristic of  $S_0 = -\Delta/T$ , which is independent of the tunneling rates, was also determined in the case of a single QD junction.<sup>20</sup> In the appendix, we derive the formula of  $S_0(T) = -\Delta/T$  for the noninteraction case when the conditions of  $t_c/k_B T \ll 1$  and  $\Gamma/k_B T \ll 1$  are satisfied. Such results imply that the behavior of  $S_0(T)$  is not sensitive to electron Coulomb interactions. This is attributed to the very small contribution of resonant channels involving electron Coulomb interactions that are far above  $E_F$ . Note that the behavior of  $S(T)$  becomes complicated if when  $E_\ell - E_F = \Delta < 0$ , because  $S(T)$  will involve many physical parameters such as electron Coulomb interactions, the electron interdot hopping strength  $t_c$ , and tunneling rate.<sup>17</sup>

To calculate the Seebeck coefficient in the nonlinear response regime, we numerically solve Eq. (5) by considering the condition of  $J = 0$ . Figure 5 shows the electrochemical potential and Seebeck coefficient as a function of temperature difference  $\Delta T$  for different detuning energies  $\Delta$  at  $k_B T_L = 40 \Gamma_0$ . The curve with triangles (considering  $\Delta = 50 \Gamma_0$ ) neglects the shift of the QD energy level yielded by the electrochemical potential. That is,  $\eta_1 = \eta_2 = 0$ .  $\Delta\mu$  increases with increasing  $\Delta T$ . When  $\Delta T > 0$ ,  $\Delta\mu = e\Delta V_a$  is negative. On the other hand,  $\Delta\mu$  is positive when  $\Delta T < 0$ . By Comparing the blue solid line with the curve with triangles in Fig. 5(a), we find that under the forward temperature bias ( $T_L > T_R$ ), the case of  $\eta_1 = \eta_2 = 0$  needs a larger electrochemical potential ( $\Delta\mu$ ) to balance diffusion carrier flow mainly through the resonant channels of  $E_0 \pm t_c$  from the left electrode to the right electrode. This is because the resonant channels are always kept in the case of  $\eta_1 = \eta_2 = 0$ . Once  $\eta_\ell \neq 0$ , the electrochemical potential will generate the off-resonant channels and the carrier diffusion flow will be blocked. Under the reverse temperature bias ( $k_B T_R > k_B T_L = 40 \Gamma_0$ ), the difference between the blue solid line and the curve with triangles is small even though  $\Delta T = -20 \Gamma_0$ . This indicates that diffusion carrier flow does increase too much with increasing temperature bias. Figure 5(b) shows the Seebeck coefficient corresponding to the electrochemical potentials shown in Fig. 5(a). The behavior shown in Fig. 5(b) can be roughly described by  $S = S_0/(1 - 0.5\Delta T/T)$ . If  $\Delta T/2T \ll 1$ , we have  $T_R = T_L - \Delta\mu/S_0$ . This result may be useful for the application of temperature detectors.<sup>22</sup>

According to the definition of  $S = (k_B/e)(-L_1/L_0)$ ,  $S$  is related to the electrical conductance  $G_e = eL_0$ . We further examined the relationship between these thermoelectric response functions. Figure 6 shows the electrical conductance ( $G_e$ ) of SCQDs with identical QDs ( $E_\ell = E_0 = E_F + 30 \Gamma_0 - eV_g$ ) as a function of gate voltage for different values of EPIs ( $\Omega_\ell$ ) at a low temperature  $k_B T = 1 \Gamma_0$ . Note that we have  $T_p = T$  in the linear response. The coupling strength of EPIs can be tuned by the phonon cavity, which modulates the phonon density

of states to change  $\lambda_\ell = \Omega_\ell/\omega_0$ .<sup>9-11)</sup> In the absence of  $\lambda_\ell = 0$ , there are eight resonant channels of  $E_0 \pm t_c$ ,  $E_0 + U_{12} \pm t_c$ ,  $E_0 + U + U_{12} \pm t_c$ , and  $E_0 + U + 2U_{12} \pm t_c$ , which are labeled from  $eV_{g1}$  to  $eV_{g8}$ . The first peak ( $eV_{g1}$ ) is shifted toward a low gate voltage with increasing  $\lambda$ , which is attributed to the shift of the QD energy level  $E_\ell^e = E_\ell - \lambda^2\omega_0$ . Because of the reduction of the interdot Coulomb interaction  $U_{\ell,j}^e = U_{\ell,j} - 2\lambda_1\lambda_2\omega_0$ , there are only six peaks and four peaks in the  $\lambda_1 = \lambda_2 = 0.5$  and  $\lambda_1 = \lambda_2 = 0.7$ . For  $\lambda_1 = \lambda_2 = 0.7$ ,  $U_{\ell,j}^e$  almost vanishes. Therefore, four peaks correspond to  $E_\ell^e \pm t_c$ , and  $E_\ell^e + U_\ell^e \pm t_c$ . For the homogenous coupling of EPIs  $\lambda_1 = \lambda_2$ ,  $t_c^e = t_c$  is independent of  $\lambda$ . The separation between the peaks corresponding to the bonding and antibonding states is invariant.

In Fig. 6, we considered the case of  $\lambda_1 > 0$  and  $\lambda_2 > 0$ . It is possible to have a positive  $\lambda_1$  and a negative  $\lambda_2$  by considering QDs at particular locations in the phonon cavity. For instance, dot A is out of phase from dot B under phonon fields [see Eq. (4)]. This will lead to a reduction of intradot Coulomb interaction and an enhancement of interdot electron Coulomb interaction. Figure 7 shows the electrical conductance ( $G_e$ ) and Seebeck coefficient ( $S_0$ ) as a function of gate voltage for different  $\lambda$  values. For  $\lambda_1 = 0.5$  and  $\lambda_2 = -0.5$ , the spectra of  $G_e$  and  $S_0$  are significantly changed owing to the reduction of interdot hopping strength [ $t_c^2 e^{-(\lambda_1 - \lambda_2)^2 \coth^2(\omega_0/(2k_B T))}$ ] and the enhancement of interdot Coulomb interactions  $U_{\ell,j} - 2\lambda_1\lambda_2\omega_0$ . The Seebeck coefficients shown in Figs. 7(c) and 7(d) correspond to Figs. 7(a) and 7(b), respectively. The Seebeck coefficient shows a change in sign arising from the bipolar effect which is electron-hole asymmetrical, where holes are defined as the empty states below the Fermi energy of electrodes.<sup>17)</sup>

#### 4. Summary and Conclusions

Intradot Coulomb interactions are more important than interdot Coulomb interactions in the observation of current rectification spectra in the Pauli spin blockade. The current rectification is not restricted in the weak interdot hopping limit ( $t_c/\Gamma \ll 1$ ). From the experimental point of view, the release from the weak interdot hopping restriction is very useful for measuring the tunneling current of SCQDs. Unlike the charge current rectification, the maximum spin-polarization current is obtained in the forward bias regime. The Seebeck coefficients in the linear and nonlinear response cases were studied. The universal behavior of the Seebeck coefficient ( $S_0 = -k_B\Delta/eT$ ) may be useful for the application of temperature detectors. EPIs provide an extra degree of freedom to control carrier transportation.

**Acknowledgments-** This work was supported by National Science Council, Taiwan, under Contract Nos. NSC 101-2112-M-008-014-MY2 and NSC 101-2112-M-001-024-MY3.

<sup>†</sup> E-mail address: mtkuo@ee.ncu.edu.tw

#### Appendix A: Seebeck coefficient

The tunneling current given by Eq. (5) can be analytically calculated by contour integration. For simplicity, this appendix only considers the case without electron Coulomb interactions.

$$J = \frac{2e\Gamma_L\Gamma_R}{h} \int d\epsilon \frac{t_c^2 [f_L(\epsilon) - f_R(\epsilon)]}{[(\epsilon - \epsilon_1 + i\Gamma_L/2)(\epsilon - \epsilon_2 + i\Gamma_R/2) - t_c^2]^2}, \quad (\text{A1})$$

$f_{L(R)}(\epsilon)$  is the Fermi distribution function of the left (right) electrode.  $\epsilon_\ell = E_\ell + \eta_\ell e\Delta V_a$ . In the linear response regime, we take  $e\Delta V_a \rightarrow 0$  and  $k_B\Delta T \rightarrow 0$  in Eq. (A1) and we have  $J = L_0 e\Delta V_a + L_1 k_B\Delta T$ , where

$$L_n/\alpha = \int_{-\infty}^{\infty} dy \frac{y^n \cos^2(y/2)}{(y - \omega_+)(y - \omega_+^*)(y - \omega_-)(y - \omega_-^*)}, \quad (\text{A2})$$

where  $\alpha = \frac{2e\Gamma_0^2 t_c^2}{4h(k_B T)^4}$ ,  $\omega_\pm = (E_\pm - E_F)/(k_B T)$ , and  $E_\pm = \epsilon_0 + i\Gamma/2 \pm E_\delta$ . We define  $\epsilon_0 = (E_1 + E_2)/2 = E_0$ ,  $\Gamma = (\Gamma_L + \Gamma_R)/2 = \Gamma_0$ , and  $E_\delta = \sqrt{((E_1 - E_2)/2)^2 + t_c^2}$ . The Seebeck coefficient is defined as  $S_0(T) = -L_1/L_0(k_B/e)$  for considering the condition of  $J = 0$ .

By using contour integration,  $L_0$  and  $L_1$  can be evaluated in terms of polygamma functions.<sup>23)</sup> Because we are interested in the case of  $k_B T/\Gamma_0 \gg 1$  and  $\Delta = (E_0 - E_F) \gg t_c$ , we have the thermoelectric response functions  $L_0$  and  $L_1$

$$L_0 = \frac{2e}{h} \frac{t_c^2}{k_B T} \frac{\pi\Gamma_0/2}{t_c^2 + (\Gamma_0/2)^2} \frac{1}{\cosh^2(\Delta/2k_B T)} \quad (\text{A3})$$

and

$$L_1 = \frac{2e}{h} \frac{t_c^2}{k_B T^2} \frac{\pi\Gamma_0/2}{t_c^2 + (\Gamma_0/2)^2} \frac{\Delta}{\cosh^2(\Delta/2k_B T)}. \quad (\text{A4})$$

On the basis of Eqs. (A3) and (A4), we obtain the electrical conductance ( $G_e$ ) and Seebeck coefficient ( $S_0$ ) with the following expressions

$$G_e = \frac{2e^2}{h} \frac{t_c^2}{k_B T} \frac{\pi\Gamma_0/2}{t_c^2 + (\Gamma_0/2)^2} \frac{1}{\cosh^2(\Delta/2k_B T)} \quad (\text{A5})$$

and

$$S_0 = \frac{-k_B\Delta}{eT}. \quad (\text{A6})$$

The Seebeck coefficient of Eq. (A6) depends on the detuning energy and equilibrium temperature.

- <sup>1)</sup> K. Ono, D. G. Austing, Y. Tokura, and S. Tarucha: Science **297** (2002) 1313.
- <sup>2)</sup> W. G. v. Wiel, S. D. Franceschi, J. M. Elzerman, T. Fujisawa, S. Tarucha, and L. Kouwenhoven: Rev. Mod. Phys. **75** (2003) 1.
- <sup>3)</sup> S. M. Huang, Y. Tokura, H. Akimoto, K. Kono, J. J. Lin, S. Tarucha, and K. Ono: Phys. Rev. Lett. **104** (2010) 136801.
- <sup>4)</sup> Q. F. Sun, Y. Xing, and S. Q. Shen: Phys. Rev. B **77** (2008) 195313.
- <sup>5)</sup> J. Fransson and M. Rasander: Phys. Rev. B **73** (2006) 205333.
- <sup>6)</sup> B. Muralidharan and S. Datta: Phys. Rev. B **76** (2007) 035432.
- <sup>7)</sup> J. Inarrea, G. Platero, and A. H. MacDonald: Phys. Rev. B **76** (2007) 085329.
- <sup>8)</sup> P. Trocha, I. Weymann, and J. Barnas: Phys. Rev. B **80** (2009) 165333.
- <sup>9)</sup> M. Trigo, A. Bruchhausen, A. Fainstein, B. Jusserand, and V. Thirry-Mieg: Phys. Rev. Lett. **89** (2002) 227402.
- <sup>10)</sup> E. M. Weig, R. H. Blick, T. Brandes, J. Kirschbaum, W. Wegscheider, M. Bichler, and J. P. Kotthaus: Phys. Rev. Lett. **92** (2004) 046804.
- <sup>11)</sup> G. Rozas, M. F. P. Winter, B. Jusserand, B. Perrin, E. Semenova, and A. Lemaître: Phys. Rev. Lett. **102** (2009) 015502.
- <sup>12)</sup> D. M. T. Kuo, S. Y. Shiau, and Y. C. Chang: Phys. Rev. B **84** (2011) 245303.
- <sup>13)</sup> D. M. T. Kuo, and Y. C. Chang: Phys. Rev. B **66** (2002) 085311.
- <sup>14)</sup> Z. Z. Chen, R. Lu, and B. F. Zhu: Phys. Rev. B **71** (2005) 165324.
- <sup>15)</sup> J. E. Ure: J. Phys. C **15** (1982) 4515.
- <sup>16)</sup> A. C. Hewson, and D. M. Newns: J. Phys. C **12**(1979) 1665.
- <sup>17)</sup> D. M. T. Kuo and Y. C. Chang: Nanoscale Res. Lett. **7** (2012) 257.
- <sup>18)</sup> P. Trocha and J. Barnas: Phys. Rev. B **85** (2012) 085408.
- <sup>19)</sup> M. Zebarjadi, K. Esfarjani, M. S. Dresselhaus, Z. F. Ren, and G. Chen, Energy Environ. Sci. **5**, (2012) 5147.
- <sup>20)</sup> D. M. T. Kuo and Y. C. Chang: Phys. Rev. B **81** (2010) 205321.

- <sup>21)</sup> D. M. T. Kuo and Y. C. Chang: Jpn. J. Appl. Phys. **49** (2010) 064301.
- <sup>22)</sup> P. Mani, N. Nakpathomkun, E. A. Hoffmann, and H. Linke: Nano Lett. **11** (2011) 4679.
- <sup>23)</sup> L. Oroszlany, A. Kormanyos, J. Cserti, and C. J. Lambert: Phys. Rev. B **76** (2007) 045318.

## Figures and Figure Captions

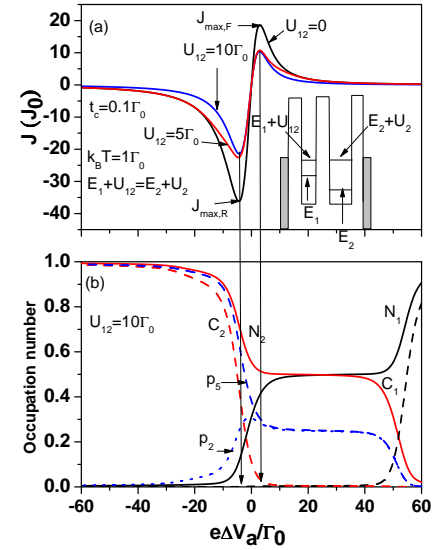


FIG. 1: (a) Tunneling current as a function of applied bias for various interdot Coulomb interactions ( $U_{12}$ ) at temperature  $k_B T = 1\Gamma_0$ . The tunneling currents are in the units of  $J_0 = 2e\Gamma_0/h$ . (b) Occupation number ( $N_\ell$ ) and two-particle correlation function ( $c_\ell$ ) in the case of  $U_{12} = 10\Gamma_0$ .

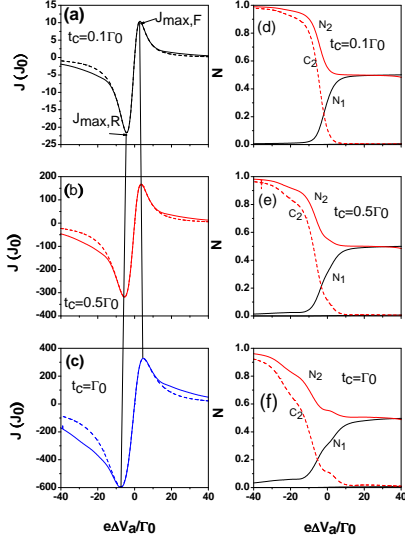


FIG. 2: Tunneling current as a function of applied bias. Diagrams (a)-(c) show the interdot hopping strengths  $t_c = 0.1, 0.5$ , and  $1 \Gamma_0$ , respectively. Diagrams (d)-(f) showing  $N$  and  $c_\ell$  correspond to diagrams (a)-(c), respectively. Note that  $c_1$  is not plotted in diagrams (d)-(f) because of the very small  $c_1$ .

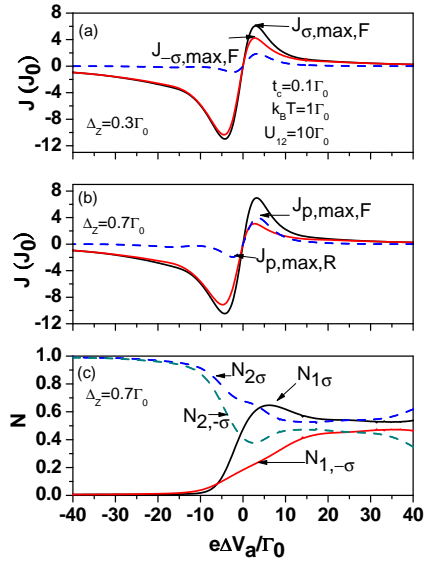


FIG. 3: Spin-dependent tunneling current as a function of applied bias: (a)  $\Delta_Z = 0.3 \Gamma_0$  and (b)  $\Delta_Z = 0.7 \Gamma_0$ .  $\Delta_Z = g\mu_B B/2$ . The spin-polarization currents (dashed lines) are defined as  $J_p = J_\sigma - J_{-\sigma}$ . (c) Spin-dependent occupation number as a function of applied bias at  $\Delta_Z = 0.7\Gamma_0$ .

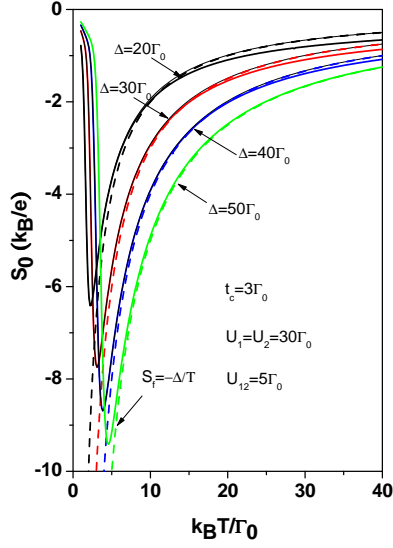


FIG. 4: Seebeck coefficient ( $S_0$ ) as a function of temperature for different detuning energies ( $\Delta = 20, 30, 40, 50 \Gamma_0$ ) in the linear response regime. The physical parameters  $U_\ell = U = 30\Gamma_0$ ,  $U_{\ell,j} = 5\Gamma_0$ ,  $\Gamma_L = \Gamma_R = \Gamma_0$ , and  $t_c = 3\Gamma_0$  are adopted. Dashed lines are calculated using  $S_f = -\Delta/T$ , which is given by Eq. (A6).

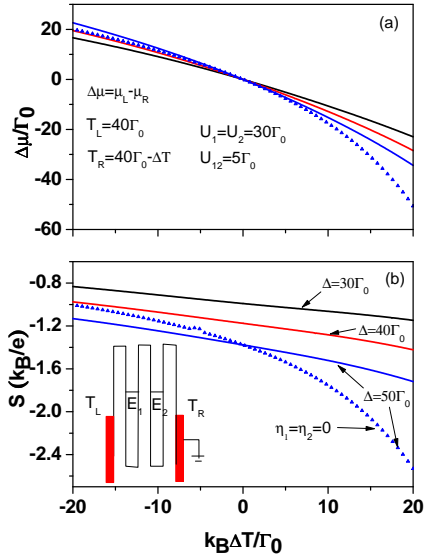


FIG. 5: (a) Electrochemical potential  $\Delta\mu$  and (b) Seebeck coefficient ( $S$ ) as a function of temperature difference  $\Delta T$  for different detuning energies at temperature of the left electrode  $T_L = 40\Gamma_0$ . Other physical parameters are the same as those in Fig. 4.



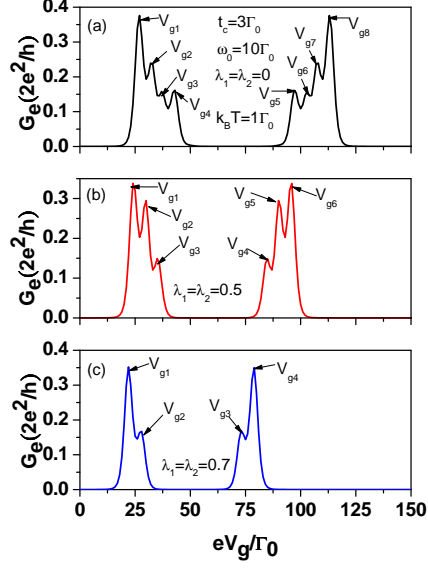


FIG. 6: Electrical conductance ( $G_e$ ) as a function of applied gate voltage for different electron-phonon interactions (EPIs) at  $k_B T = 1\Gamma_0$ ,  $E_\ell = 30\Gamma_0 - eV_g$ ,  $U_\ell = 60\Gamma_0$ , and  $U_{\ell,j} = 10\Gamma_0$ . Diagrams (a)-(c) show the results for  $\lambda_1 = \lambda_2 = 0, 0.5$ , and  $0.7$ , respectively

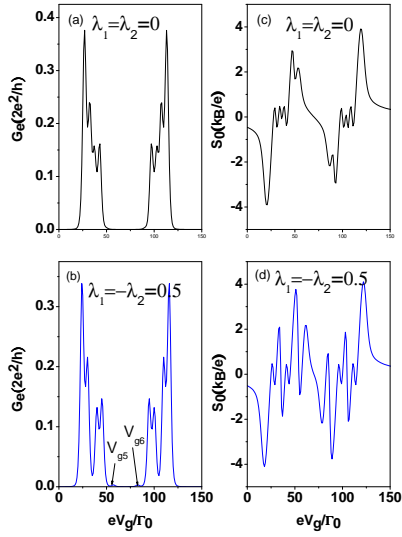


FIG. 7: (a)-(b) Electrical conductance ( $G_e$ ) and (c)-(d) Seebeck coefficient ( $S_0$ ) as a function of applied gate voltage for different EPIs at  $k_B T = 1\Gamma_0$ . Solid lines:  $\lambda_1 = \lambda_2 = 0$ , dashed lines:  $\lambda_1 = -\lambda_2 = 0.5$ . Other physical parameters are the same as those in Fig. 6.